

Full nonlinear closure for a hydrodynamic model of transport in silicon

M. Trovato and P. Falsaperla

Dipartimento di Fisica, Università di Catania, Corso Italia 57, 95129 Catania, Italy

(Received 8 September 1997)

We derive, using the entropy maximum principle, an expression for the distribution function of carriers as a function of a set of macroscopic quantities (density, velocity, energy, deviatoric stress, heat flux). Given the distribution function, we can obtain a hydrodynamic model in which all the constitutive functions (fluxes and collisional productions) are explicitly computed starting from their kinetic expressions. We have applied our model to the simulation of the thermodynamic properties of bulk silicon and of some n^+nn^+ submicrometer Si devices (with several doping profiles and applied biases), obtaining results comparable with Monte Carlo simulations. Computation times are of order of few seconds for a picosecond of simulation. [S0163-1829(98)01607-5]

I. INTRODUCTION

The increasing miniaturization of modern electronic devices requires an accurate modelization of transport in semiconductors. This is of great importance for describing phenomena such those due to hot electrons, i.e., the conditions very far from thermodynamic equilibrium caused by strong electric fields and field gradients.

The most general approach to the simulation of charge transport in semiconductors employs the semiclassical Boltzmann transport equation (BTE) coupled with Poisson equation. A numerical solution of such system of equations with traditional techniques is extremely complex, and then approximate methods based on kinetic and fluid dynamic (FD) models are often preferred.

The most accurate kinetic description is given by Monte Carlo (MC) methods, which can take into account explicitly both the band structure and the various scattering phenomena.^{1,2} This method permits us to compute directly all the quantities relative to transport (such as the distribution function, density of carriers, velocity, mean energy, and so on) but at a cost of long computation times and stochastic noise in data. The results obtained from MC simulations permit us also to calculate *transport coefficients*, which are used as an input to more simplified FD models. Other kinetic approaches are based on the choice of particular forms of the nonequilibrium distribution function of carriers. Common examples are the simple shifted Maxwellian³ or an expansion of the distribution in spherical harmonics.⁴ The cylindrical symmetry constraint in momentum space and the reduced number of terms of the expansion that can be practically used do not permit, however, to describe transport properties of carriers in conditions very far from equilibrium.⁵

The FD models are obtained considering a set of moments of the BTE. Such models clearly need the knowledge of *constitutive functions* (fluxes and collisional productions) present in the hierarchy of equations. For instance, the most common hydrodynamic models^{6,8-13} use the dynamic variables: *numerical density* n , *velocity* \vec{v} , and *energy density* W with some *ad hoc* constitutive equations for the *heat flux* and the *stress tensor* of type Navier-Stokes-Fourier and a modelization for the collisional productions through relaxation

times, which, for small departures from equilibrium, contrasts with the Onsager reciprocity relations.¹⁴ The main defects of these FD models depend, then, on the constitutive equations, which are usually fixed on a phenomenological basis, introducing free parameters, such as relaxation times and transport coefficients, which have an unknown dependence on the geometry and working conditions of the simulated devices. The presence of these *free parameters*⁶ has always been a limit to a practical use of FD models, because, in general, such parameters are determined in each case on the basis of MC simulations or experimental data.

We have developed a hydrodynamic (HD) model⁷ for the simulation of transport phenomena in semiconductors, based on extended thermodynamics and on the entropy maximum principle (EMP). In this model, besides the usual quantities $\{n, nv_i, W\}$, also the *energy flux density* S_i and the *traceless part of momentum flux density* $\Sigma_{\langle ij \rangle}$ ¹⁵ are considered dynamic variables and they satisfy further balance equations. We have then, as independent variables, the first thirteen moments of the distribution function $F_A = \{n, nv_i, W, \Sigma_{\langle ij \rangle}, S_i\}$. Following the EMP we express the distribution function through the set of moments F_A as $\mathcal{F}(\vec{k}, \vec{r}, t) = \mathcal{F}[F_A(\vec{r}, t), \vec{k}]$. This distribution turns out to be a strongly nonlinear function of the moments. Given the distribution, we can determine the unknown constitutive functions appearing in the hierarchy of the equations that describes the time evolution of the moments. We point out that the computation of collisional productions is then based on the sole knowledge of the scattering kernels and the physical quantities they contain. Our HD model is then fully closed, and, contrarily to other HD models, does not contain any *free parameter*. On the other hand, the distribution function we obtain has no particular symmetry restrictions and is fully suitable for three-dimensional models. Its strong nonlinearity is capable of describing transport phenomena even in conditions far from thermodynamic equilibrium, as those present in submicron devices with very high electric fields and field gradients [$E \approx 10^5$ V/cm, $E/(dE/dx) \approx 100$ Å].

We remark that in our paper the EMP is used in a different way with respect to most of the previous applications (see Ref. 16), in that our method leads to a dynamical description of the physical system. The EMP, by itself, does

not provide any information about the dynamic evolution of a system, but gives only a criterion to express the nonequilibrium distribution function as function of a set of macroscopic quantities, used as constraints. In this paper both the distribution function and the macroscopic quantities are regarded as local quantities, functions of position and time. To obtain a dynamic model it is necessary to know a set of evolution equations for the constraints, which include an accurate description of the microscopic collisional processes. So, in our application of the EMP, we can see two steps: (a) determine a general and *analytic* expression for the distribution function, as function of the macroscopic quantities used as constraints; (b) starting from the Boltzmann transport equation, obtain a set of equations for the constraints that represents a completely *closed* hydrodynamic model in which all the constitutive functions are completely determined starting from their kinetic expressions.

Then we can say that our use of the EMP depends both on the choice of a set of constraints (moments of the distribution function) and on the determination of a set of evolution equations for these constraints that takes explicitly into account the underlying physical processes (the various scattering phenomena, in this case). Only by knowing the dynamic evolution of the macroscopic quantities used as constraints it is possible to determine the correct dynamic evolution of the distribution function in phase space.

The plan of this paper is the following. In Sec. II we introduce the balance equations for the charged carriers and describe the physical characteristics of the model. In Sec. III we exploit the EMP in order to obtain an analytic expression for the distribution function. In Sec. IV we analyze the restriction of the model to the one-dimensional case giving explicitly both the set of balance equations for the moments F_A and the expression of the constitutive functions (fluxes and collisional productions). In Sec. V we discuss the results of the simulations of bulk silicon and unipolar n^+nn^+ devices with different doping profiles, size of the active regions, and applied bias. In Sec. VI we analyze the system of equations and its hyperbolicity domain. In Sec. VII we discuss briefly a generalization of the Nessyahu-Tadmor numerical scheme to nonhomogeneous systems and its applicability to our case.

II. PHYSICAL CHARACTERISTICS OF THE MODEL

We consider here a HD model for transport phenomena in silicon. Our main purpose in the development of this model, has been to test how accurately our distribution function describes strong nonequilibrium conditions. Therefore we have used a simplified band structure. As is well known, electrons contributing to transport are mainly those belonging to the six equivalent X valleys which, up to an energy of about 0.5 eV, can be considered approximately parabolic. Electrons can then be described by a density of states effective mass $m^* = 0.32m_e$ and a band energy $\varepsilon(\vec{k}) = \hbar^2 k^2 / 2m^*$. In the same energy range, the main scattering phenomena are due to electron-phonon interactions, which produce intervalley and intravalley transitions.²

We will consider intervalley transitions caused both by f -type and g -type phonons. The scattering probability per unit time for intervalley transitions of an electron from state

\vec{k} to state \vec{k}' can be expressed as

$$S_\eta(\vec{k}, \vec{k}') = Z_\eta \frac{\pi \Delta_\eta^2}{V \rho \omega_\eta} \left[\frac{N_\eta}{N_\eta + 1} \right] \delta[\varepsilon(\vec{k}') - \varepsilon(\vec{k}) \mp \hbar \omega_\eta],$$

with $\eta = g_1, g_2, g_3, f_1, f_2, f_3$. (1)

Here Z_η is the number of possible final equivalent valleys ($Z_\eta = 1$ for $\eta = g_1, g_2, g_3$ and $Z_\eta = 4$ for $\eta = f_1, f_2, f_3$), Δ_η is the coupling constant, V is the crystal volume, ρ is the Si density, ω_η is the phonon angular frequency, $N_\eta = 1 / [\exp(\hbar \omega_\eta / K_B T_0) - 1]$ is the phonon occupation number (with T_0 the lattice temperature), while the upper and the lower option in the expression corresponds to absorption and emission, respectively.

For intravalley transitions we will consider scattering with acoustic phonons, which will be regarded as approximately elastic. Since in this approximation there is no distinction between final states obtained by absorption or emission processes, we can express the sum of the intravalley transitions probabilities as

$$S_{ac}(\vec{k}, \vec{k}') = \frac{2\pi K_B T_0 E_l}{V \hbar \rho U_l^2} \delta[\varepsilon(\vec{k}') - \varepsilon(\vec{k})],$$
 (2)

being K_B the Boltzmann constant, U_l the longitudinal sound velocity, E_l the deformation potential for longitudinal acoustic phonons. For the values of all the constants appearing in the scattering terms (1),(2) we have used the parameters reported in Ref. 2.

We consider the BTE for an electron gas

$$\frac{\partial \mathcal{F}(\vec{k}, \vec{r}, t)}{\partial t} + \frac{dx_i}{dt} \frac{\partial \mathcal{F}(\vec{k}, \vec{r}, t)}{\partial x_i} - \frac{e}{\hbar} E_i \frac{\partial \mathcal{F}(\vec{k}, \vec{r}, t)}{\partial k_i} = Q(\mathcal{F}),$$
 (3)

where $\mathcal{F} = \mathcal{F}(\vec{k}, \vec{r}, t)$ is the single-particle Boltzmann distribution function, $dx_i/dt = \hbar k_i / m^*$ is the electron group velocity and $Q(\mathcal{F})$:

$$Q(\mathcal{F}) = \frac{V}{(2\pi)^3} \int d\vec{k}' S(\vec{k}', \vec{k}) \mathcal{F}(\vec{k}', \vec{r}, t) - \frac{V}{(2\pi)^3} \int d\vec{k} S(\vec{k}, \vec{k}') \mathcal{F}(\vec{k}, \vec{r}, t)$$
 (4)

is the collisional production due to the different scattering processes [$Q_\eta(\mathcal{F})$ for the intervalley transitions and $Q_{ac}(\mathcal{F})$ for the intravalley transitions].

We can pass from the Boltzmann equation (3) to the hydrodynamic equations of the first thirteen moments considering the following *kinetic quantities* (see Ref. 15)

$$\psi_A(\vec{k}) = \left\{ 1, \frac{\hbar}{m^*} k_i, \frac{\hbar^2}{2m^*} k^2, \frac{\hbar^2}{m^*} k_{\langle i} k_{j \rangle}, \frac{\hbar^3}{2(m^*)^2} k^2 k_i \right\}.$$

Multiplying Eq. (3) by $\psi_A(\vec{k})$ and integrating in \vec{k} space we obtain the balance equations for the following *moments of the distribution function* or *macroscopic fields*: density of carriers n , flux of carriers nv_i , total energy density W , traceless part of momentum flux density $\Sigma_{\langle ij \rangle}$, energy flux density S_i , being

$$W = \frac{3}{2}p + \frac{1}{2}nm^*v^2, \quad \Sigma_{\langle ij \rangle} = \sigma_{\langle ij \rangle} + nm^*v_{\langle i}v_{j \rangle},$$

$$S_i = q_i + \sigma_{\langle ij \rangle}v_j + \frac{5}{2}pv_i + \frac{1}{2}nm^*v^2v_i,$$

where v_i is the mean velocity, $p = nK_B T$ is the pressure, $\sigma_{\langle ij \rangle}$ is the nonconvective part of tensor $\Sigma_{\langle ij \rangle}$ and q_i is the heat flux. If we denote this set of moments by $F_A = \{n, nv_i, W, \Sigma_{\langle ij \rangle}, S_i\}$, we can write

$$F_A = \int \psi_A(\vec{k}) \mathcal{F}(\vec{k}, \vec{r}, t) d\vec{k} \quad (5)$$

and the generic balance equation is then

$$\frac{\partial F_A}{\partial t} + \frac{\partial F_{Ak}}{\partial x_k} = R_A + P_A + \tilde{P}_A. \quad (6)$$

Here R_A denotes the production term due to the electric field, while the fluxes and collisional productions $\{P_A, \tilde{P}_A\}$ caused by intravalley and intervalley transitions are, respectively,

$$\begin{aligned} F_{Ak} &= \frac{\hbar}{m^*} \int \psi_A(\vec{k}) k_k \mathcal{F}(\vec{k}, \vec{r}, t) d\vec{k}, \\ P_A &= \sum_{\eta} \int \psi_A(\vec{k}) Q_{\eta}(\mathcal{F}) d\vec{k}, \\ \tilde{P}_A &= \int \psi_A(\vec{k}) Q_{ac}(\mathcal{F}) d\vec{k}. \end{aligned} \quad (7)$$

The set of balance equations (6) contains several unknown functions, i.e., the fluxes of the equations for $\Sigma_{\langle ij \rangle}$ and S_i , and the collisional productions $\{P_A, \tilde{P}_A\}$. The system can then be *closed* if the unknown constitutive functions $H_A = \{P_A, \tilde{P}_A, F_{Ak}\}$ can be expressed by means of the fields F_A . This problem can be solved with the help the variational method known as *entropy maximum principle*,^{18–23} which allows the determination of the non-equilibrium distribution function of hot carriers and consequently permits to find a closure for the *constitutive functions*. We will show (by a comparison with MC simulations performed under the same physical approximations) that in this way it is possible to describe accurately some simple Si devices even in conditions very far from thermodynamic equilibrium.

III. MAXIMIZATION OF ENTROPY

We start from the known expression of entropy density $h = -C \int \mathcal{F} \log(\mathcal{F}) d\vec{k}$ (where C is a constant) assuming that $\mathcal{F}(\vec{k}, \vec{r}, t)$ depends on \vec{r} and t only through the fields $F_A(\vec{r}, t)$ and then we determine the distribution function, of the form $\mathcal{F}(\vec{r}, \vec{k}, t) = \mathcal{F}[F_A(\vec{r}, t), \vec{k}]$ that maximizes h under the constraints that the moments F_A are expressed by the relations (5). Following this procedure, we maximize the functional

$$h' = h - \sum_{A=1}^{13} \Lambda_A \left[\int \psi_A(\vec{k}) \mathcal{F}(\vec{r}, \vec{k}, t) d\vec{k} - F_A \right], \quad (8)$$

imposing $\delta h' = 0$. The quantities Λ_A are the *Lagrange multipliers* associated with the constraint equations (5). As is well known, the distribution function obtained with this procedure^{16–23} assumes the following form

$$\mathcal{F} = \exp(-\Sigma), \quad \Sigma = \sum_{A=1}^{13} \psi_A \Lambda_A. \quad (9)$$

To obtain an explicit expression of \mathcal{F} we have yet to express the multipliers Λ_A as function of the constraints, i.e., the moments F_A . By inserting Eq. (9) into the definition of fields (5) we have $F_A = F_A(\Lambda_B)$, and so, to determine \mathcal{F} , we must invert this latter relations obtaining $\Lambda_A = \Lambda_A(F_B)$. This inversion is extremely difficult and can be obtained only by numerical integration or by a series expansion of \mathcal{F} .²⁴ We have followed the latter approach, expanding \mathcal{F} to third order in $\{v_i, \sigma_{\langle ij \rangle}, q_i\}$ around an equilibrium configuration defined by a local Maxwellian \mathcal{F}_M . The choice of a local Maxwellian is justified by the following observation. It is known¹⁴ that energy W reaches its equilibrium value much more slowly than other moments such as $\{v, \sigma, q\}$, because many collision processes (mainly with acoustic phonons involved in intravalley transitions) are almost elastic. This fact implies that during the relaxation process that leads to a global thermodynamic equilibrium (in which $v = \sigma = q = 0$, and $T = T_0$) the carriers will reach a partial thermodynamic equilibrium (in which $v = \sigma = q = 0$, but $T \neq T_0$) corresponding to the local Maxwellian (around which we have computed the expansion)

$$\mathcal{F}_M = n \left(\frac{\hbar^2}{2\pi m^* K_B T} \right)^{3/2} \exp\left(\frac{-\varepsilon(\vec{k})}{K_B T} \right),$$

which contains the quantities $n = n(\vec{r}, t)$, and $T = T(\vec{r}, t)$ as functions of position and time. Introducing the series expansion of \mathcal{F} into Eq. (5) all the quadratures can be done analytically, and the resulting relations can be inverted. In this way we can express \mathcal{F} as a strongly nonlinear function of $m_A = \{n, p, v_i, \sigma_{\langle ij \rangle}, q_i\}$.

In the specific case of semiconductors we will show that by using this distribution function we can obtain results comparable with the results of MC simulations with a remarkable reduction of the computation times.

IV. ONE-DIMENSIONAL HYDRODYNAMIC MODEL

The model resulting from the procedure described in the previous sections is fully three dimensional, but we show here one-dimensional results. The only independent variables are in this case $F_A = \{n, nv_x = nv, W, \Sigma_{\langle xx \rangle} = \Sigma, S_x = S\}$, (analogously $m_A = \{n, p, v = v_x, \sigma = \sigma_{\langle xx \rangle}, q = q_x\}$ and $E = E_x$) satisfying the following balance equations

$$\begin{aligned} \frac{\partial n}{\partial t} + \frac{\partial nv}{\partial x} &= 0, \\ \frac{\partial nv}{\partial t} + \frac{1}{m^*} \frac{\partial(\Sigma + \frac{2}{3}W)}{\partial x} &= -\frac{neE}{m^*} + P_{nv} + \tilde{P}_{nv}, \end{aligned} \quad (10)$$

$$\frac{\partial W}{\partial t} + \frac{\partial S}{\partial x} = -nveE + P_w,$$

$$\begin{aligned} \frac{\partial \Sigma}{\partial t} + \frac{\partial}{\partial x} \left(\frac{2}{3} nm^* v^3 + \frac{4}{3} p v + \frac{7}{3} \sigma v + \frac{8}{15} q + G_\Sigma \right) \\ = -\frac{4}{3} n v e E + P_\Sigma + \tilde{P}_\Sigma, \end{aligned}$$

$$\begin{aligned} \frac{\partial S}{\partial t} + \frac{\partial}{\partial x} \left(\frac{1}{2} nm^* v^4 + \frac{16}{5} q v + 4 p v^2 + \frac{5}{2} \sigma v^2 + G_S \right) \\ = -e E \left(\frac{3}{2} n v^2 + \frac{5 p}{2 m^*} + \frac{\sigma}{m^*} \right) + P_S + \tilde{P}_S, \end{aligned}$$

being $P_A = \{P_{nv}, P_w, P_\Sigma, P_S\}$ and $\tilde{P}_A = \{\tilde{P}_{nv}, 0, \tilde{P}_\Sigma, \tilde{P}_S\}$ the collisional production terms due, respectively, to intervalley and intravalley transitions while $G_A = \{G_S, G_\Sigma\}$ are the constitutive functions present in fluxes. Considering the expansion (to third order in the fields $\{v, q, \sigma\}$) of $\mathcal{F}(m_A, \vec{k})$ around equilibrium configuration (in which $v = \sigma = q = 0$) defined by a local Maxwellian distribution, we find for functions G_Σ, G_S the relations

$$\begin{aligned} G_\Sigma &= \left(\frac{36}{25} \frac{1}{p} q \sigma \right) + \left(\frac{272}{625} \frac{nm^*}{p^3} q^3 - \frac{99}{125} \frac{1}{p^2} q \sigma^2 \right), \\ G_S &= \frac{5}{2} \frac{p^2}{nm^*} + \frac{7}{2} \frac{p}{nm^*} \sigma + \left(\frac{1}{nm^*} \sigma^2 + \frac{74}{25} \frac{1}{p} q^2 \right) \\ &\quad + \left(\frac{158}{125} \frac{1}{p^2} q^2 \sigma + \frac{36}{25} \frac{1}{p} v q \sigma \right). \end{aligned} \quad (11)$$

Analogously, starting from expressions for scattering probabilities (1),(2) and using relations (7) we find, for the intravalley transitions,

$$\tilde{P}_{nv} = -\frac{4}{15} \xi \frac{n^2}{p^2} \tilde{A}, \quad \tilde{P}_\Sigma = -\frac{16}{25} \xi \frac{nm^*}{p^2} \tilde{C}, \quad \tilde{P}_S = -\frac{12}{5} \xi \tilde{D}, \quad (12)$$

with

$$\xi = \frac{E_l^2 K T_0}{\hbar^4 \rho U_l^2} \left(\frac{2m^*}{\pi} \right)^{3/2} \left(\frac{p}{n} \right)^{1/2},$$

and, for intervalley transitions,

$$\begin{aligned} P_{nv} &= \frac{4}{3} \sum_\eta \mathcal{A}_\eta \sum_{i=1}^5 A_{2i+1} [(N_\eta + 1) H_{2i+1}^+ + N_\eta H_{2i+1}^-], \\ P_w &= \sum_\eta \mathcal{A}_\eta X_\eta \sum_{i=0}^4 B_{2i+1} [(N_\eta + 1) H_{2i+1}^+ - N_\eta H_{2i+1}^-], \\ P_\Sigma &= \frac{4}{15} \sum_\eta \mathcal{A}_\eta \sum_{i=2}^5 C_{2i+1} [(N_\eta + 1) H_{2i+1}^+ + N_\eta H_{2i+1}^-], \\ P_S &= \frac{4}{3} \sum_\eta \mathcal{A}_\eta \sum_{i=2}^6 D_{2i+1} [(N_\eta + 1) H_{2i+1}^+ + N_\eta H_{2i+1}^-], \end{aligned} \quad (13)$$

with

TABLE I. Devices parameters.

Device	N^+ (cm^{-3})	N (cm^{-3})	Channel (μm)	x_s (μm)	bias (V)
A	10^{18}	10^{16}	0.2	0.01	1
B	10^{18}	10^{16}	0.3	0.01	1
C	$5 \cdot 10^{17}$	$2 \cdot 10^{15}$	0.4	0.01	1-2
D	$5 \cdot 10^{17}$	$2 \cdot 10^{15}$	0.4	0.04	2
E	$5 \cdot 10^{17}$	$2 \cdot 10^{15}$	0.4	0.06	2

$$\mathcal{A}_\eta = -\frac{n}{\hbar^3} \left(\frac{m^* n}{2\pi p} \right)^{3/2} \frac{\Delta_\eta^2}{\rho \omega_\eta} Z_\eta X_\eta, \quad X_\eta = \frac{\hbar \omega_\eta n}{2 p},$$

where all the physical constants are those previously defined for the scattering probabilities $S_{ac}(\vec{k}, \vec{k}')$, $S_\eta(\vec{k}, \vec{k}')$. The dimensionless quantities H_{2i+1}^\pm can be expressed by means of the modified Bessel functions K_1 and K_2 . Defining $G^\pm = X_\eta \exp(\mp X_\eta) K_2(X_\eta)$ we have

$$\begin{aligned} H_1^\pm &= \exp(\mp X_\eta) K_1(X_\eta), \quad H_3^\pm = \pm H_1^\pm + G^\pm, \\ H_{2i+1}^\pm &= \pm 2 H_{2i-1}^\pm \pm (i+1)! \left[\sum_{n=1}^{i-2} \frac{3 H_{2n+1}^\pm}{(n+3)!} \pm \frac{G^\pm}{2} \right], \\ &\quad i=2, \dots, 6, \end{aligned}$$

while all the coefficients $\{\tilde{A}, \tilde{C}, \tilde{D}\}$ and $\{A_{2i+1}, B_{2i+1}, C_{2i+1}, D_{2i+1}\}$ present in the production terms (12) and (13) turn out to be very complex polynomial functions of the moments m_A . We report integrally the coefficients in Appendix A, notwithstanding their complexity, because the resulting closure is of general value in the simulation of unipolar devices. Analyzing these coefficients we observe that, as we should expect, at local thermodynamic equilibrium ($v = \sigma = q = 0$) all collisional productions vanish, except for P_w , which vanishes only at global equilibrium ($T = T_0$).

V. DEVICE SIMULATIONS

As test cases, we have considered bulk Si and five unipolar and one-dimensional devices n^+nn^+ (labeled A, B, C, D, E) at different doping and applied biases, as summarized in Table I. The sample n^+nn^+ devices have regions n^+ of length $0.1 \mu\text{m}$ and a channel n , respectively, of length $0.2 \mu\text{m}$ (device A), $0.3 \mu\text{m}$ (device B) and $0.4 \mu\text{m}$ (devices C, D, and E). The lattice temperature T_0 is 300 K and the doping profile $N(x)$ has been smoothed at junction points $x_1 = 0.1 \mu\text{m}$ and $x_2 = 0.3 \mu\text{m}$, $0.4 \mu\text{m}$, and $0.5 \mu\text{m}$ (for the different devices) with a properly scaled erfc function, i.e.,

$$N(x) = N + \frac{1}{2} (N^+ - N) \left\{ 2 + \operatorname{erfc} \left[\frac{x - x_1}{x_s} \right] - \operatorname{erfc} \left[\frac{x - x_2}{x_s} \right] \right\},$$

where $x_s = 0.01 \mu\text{m}$, $0.04 \mu\text{m}$, and $0.06 \mu\text{m}$ as reported in Table I. Boundary conditions are obtained by imposing null gradient to all moments at boundary points.²⁵ These conditions seem compatible with the effective configuration of moments, both in transient and in the final stationary state. For all the device simulations reported in this paper we have

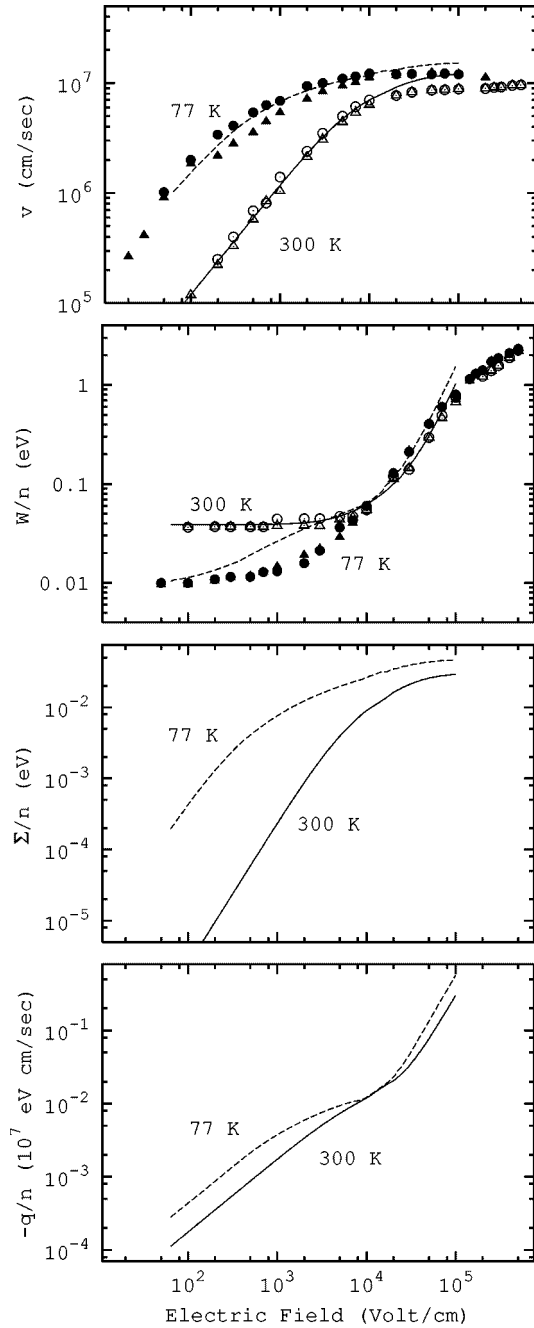


FIG. 1. HD simulation of bulk silicon. Velocity, energy, traceless momentum flux, and heat flux (with sign changed) as functions of the applied electric field at temperatures of 300 K (solid lines) and 77 K (dashed lines). For the mean energy and velocity we report also MC data (from Ref. 27) of full-band simulations with electric fields directed along the $\langle 100 \rangle$ (triangles) and the $\langle 111 \rangle$ (circles) crystallographic directions.

used the finite differences numerical scheme described in Sec. VII, with $N_c = 130$ cells and a time step $k = 0.0016$ ps for a total time of 5 ps. In these conditions our code requires about two seconds for a picosecond of simulation on a AlphaStation 600, 333 MHz. MC device simulations have been performed with the DAMOCLES code,²⁶ using 15 000 particles and under the same physical approximations of our HD model [parabolic isotropic bands and same values (see Ref. 2) of the collisional kernels parameters].

Figure 1 shows the values, for bulk silicon, of velocity,

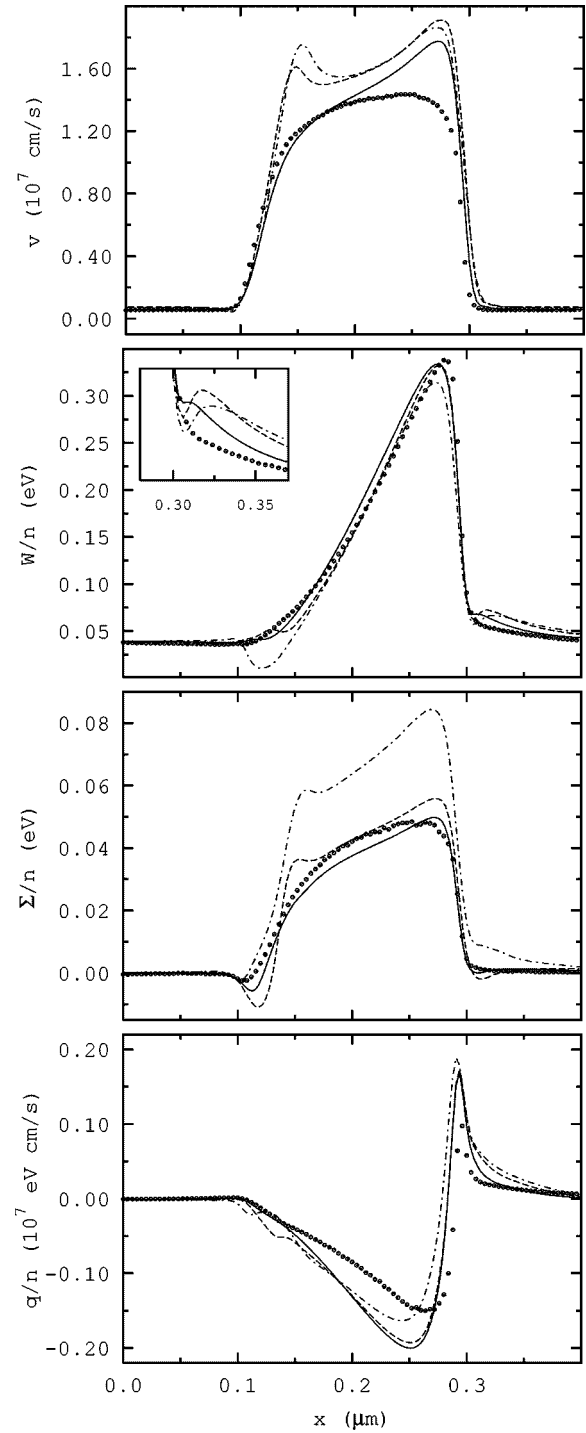


FIG. 2. Field values as a function of position for device A. Points are MC data. Lines are from the present HD model with closures for collisional productions at, respectively, first (dash-dotted lines), second (dashed lines), and third (solid lines) order.

energy, the traceless part of the momentum flux density, and heat flux, as functions of the applied electric field (at lattice temperatures $T_0 = 300$ K and $T_0 = 77$ K). We report also a comparison with MC simulations²⁷ for velocity and mean energy. These MC simulations have been performed using a full band model and for two orientations of the electric field (along the $\langle 100 \rangle$ and $\langle 111 \rangle$ directions). We note some discrepancy, for low values of the electric field, in the curve of mean energy at $T_0 = 77$ K. This is probably imputable to the

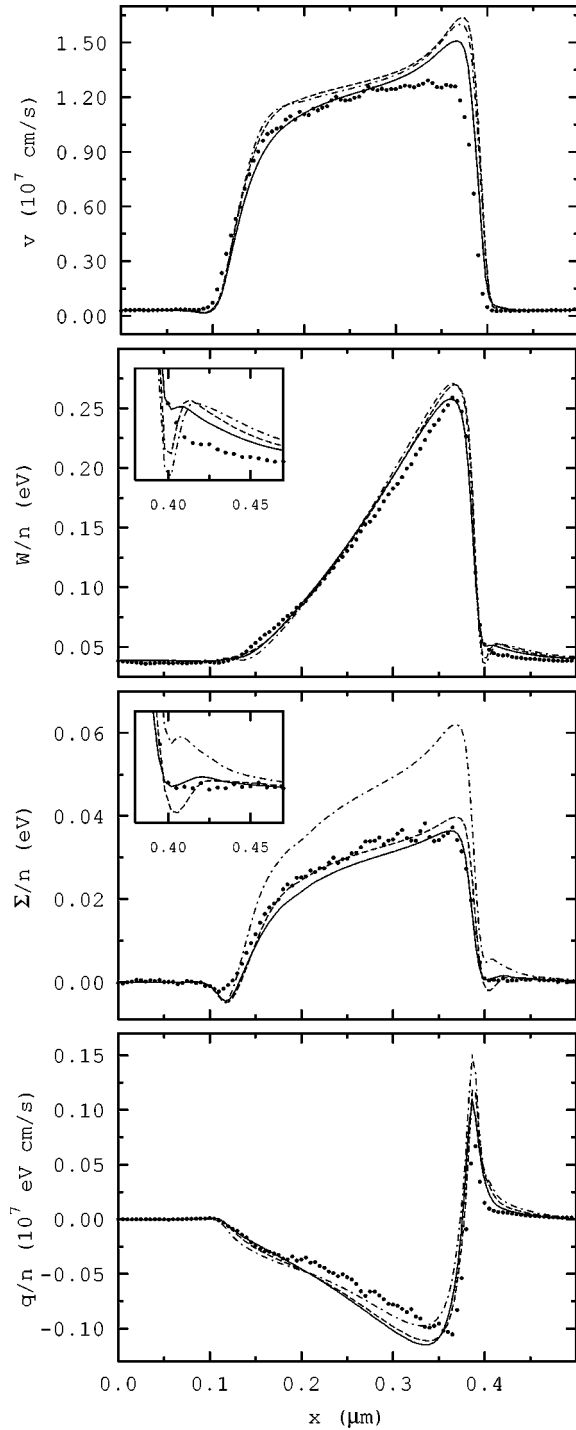


FIG. 3. Same quantities as for Fig. 2 for device *B*.

simplified description of acoustic scattering, that we have considered, for intravalley transitions, as an elastic process. This approximation can be effectively used at high fields and/or high temperatures but will fail at low fields and temperatures in that the maximum transferred energy will be no longer a small fraction of the kinetic energy of electrons.² We observe also that for high values of the electric field our results differ from MC because of the different model used for the band structure.

Figures 2, 3, and 4 show velocity, energy, the traceless part of the momentum flux density, and heat flux for devices *C*, *B*, and *C* (with a bias of 1 V). In Figs. 2 and 3 we report

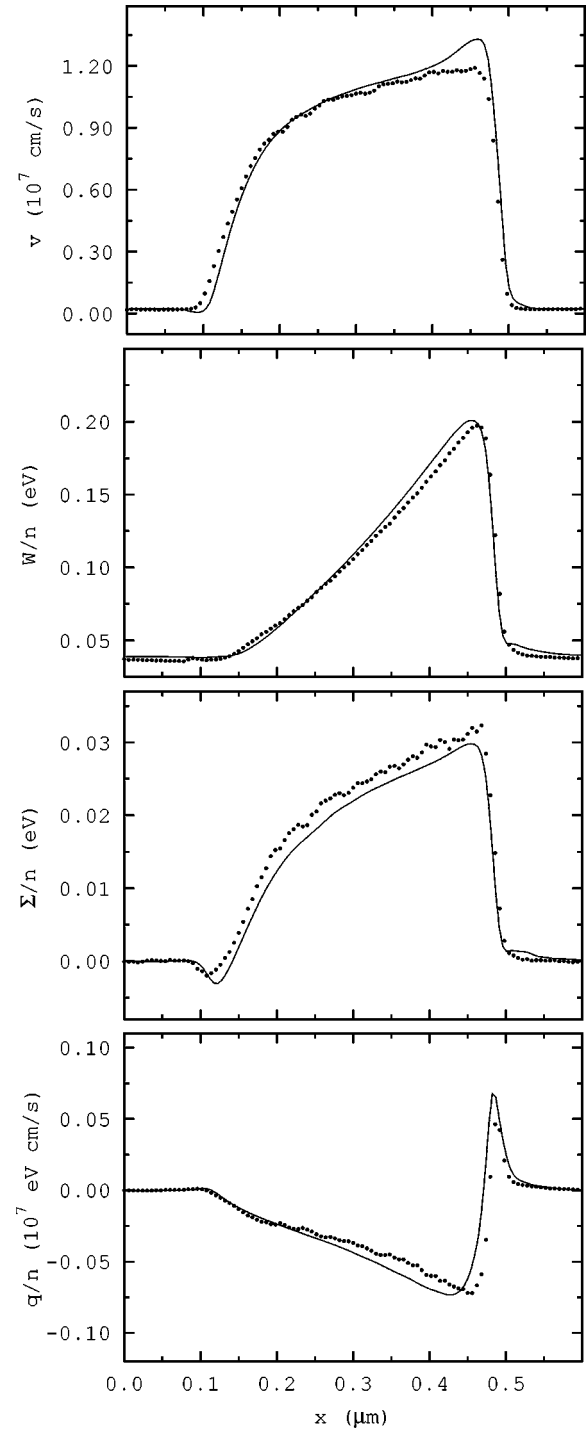


FIG. 4. Field values as function of position for device *C* with a 1 V bias. Points are MC data. Lines are from the present HD model.

the results of a series of simulations for devices *A* and *B* with three different closures, in which the collisional productions are evaluated, respectively, with a first-, second-, and third-order expansion. We see that for devices with such high fields and field gradients a strongly nonlinear description is necessary to obtain a good agreement with MC simulations.

In Figs. 5 and 6 we report velocity, energy, the traceless part of the momentum flux density, heat flux, doping profiles, and electric fields for devices *C* (with a bias of 2 V), *D* and *E*.

As an overall comment to Figs. 2–6, we observe that

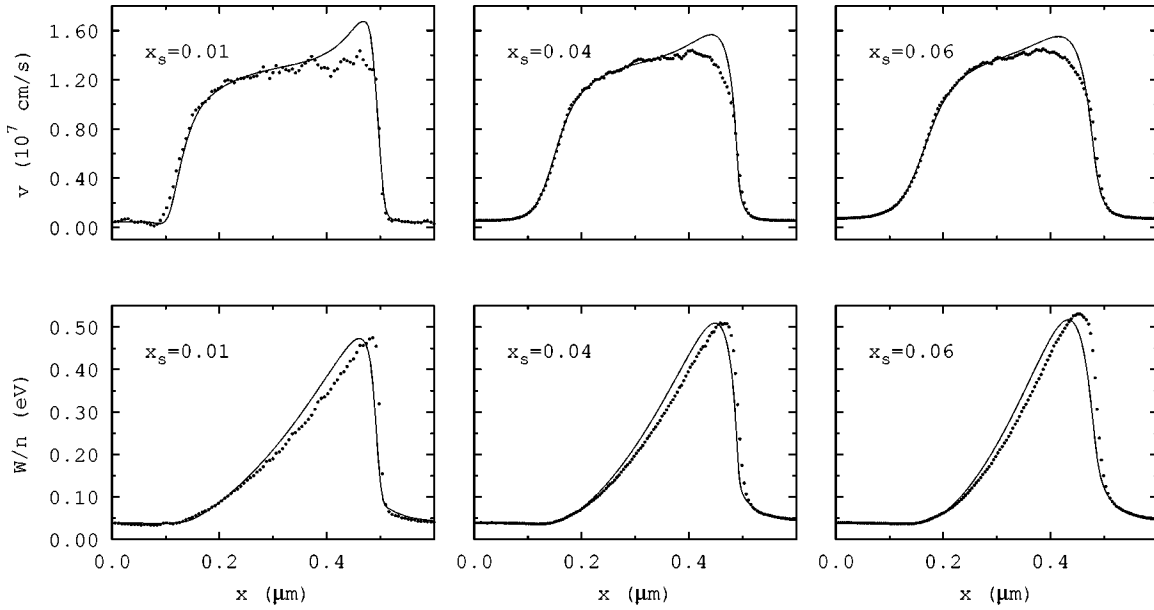


FIG. 5. Velocity and energy for devices *C*, *D*, and *E* with a 2 V bias. Solid lines are from HD simulation, points are from MC. The devices differ only in the smoothing parameter used for the doping profile (see Table I). These simulations show, near the second junction, the strong influence of the electric field gradients (see Fig. 6) on the HD simulation.

overshoot velocity pick, presented by the devices in proximity to the second junction, tends to decrease both with a better description of collisional productions (higher-order expansion in devices *A* and *B*) and with lower gradients of the electric field (devices *D* and *E*).

In Fig. 7 we show the *current density-bias* characteristic curves for devices *C*, *D*, and *E*.

Figure 8 shows the time evolution of velocity, energy, the traceless part of the momentum flux density, and heat flux, as functions of position for device *C* with a 1 V bias. We see that all the fields are nearly relaxed after 4 ps of evolution.

In the case of one-dimensional devices the distribution function presents a cylindrical symmetry in \vec{k} space, and then can be conveniently represented as function of k_x and $k_t = (k_y^2 + k_z^2)^{1/2}$ (see Appendix B). We show in Figs. 9 and 10 the function

$$f(k_x, k_t, x, t) = 2\pi k_t \mathcal{F}(k_x, k_t, m_A), \quad (14)$$

normalized such that

$$\int f(k_x, k_t, x, t) dk_x dk_t = 1$$

at different locations in device *C*. Note that because of collisional processes a fraction of the electron population seems to relax toward an equilibrium condition (i.e., a Maxwellian distribution centered at $k_x = k_t = 0$). This phenomenon is more evident in the simulation with an applied bias of 2 V [Fig. (10)]. In this case the electric field has the highest values and then the nonrelaxed fraction of electrons has a higher mean value of \vec{k} .

Integrating the maximum entropy distribution function in \vec{k} space with respect to the solid angle $d\Omega$, we obtain the electron energy distribution (see Appendix B) in the form

$$f(\varepsilon(k), m_A(x, t)), \quad \text{such that} \quad \int f(\varepsilon, m_A(x, t)) d\varepsilon = 1. \quad (15)$$

Figures 11, 12, and 13 show the electron energy distribution as a function of position and energy for devices *A*, *B*, and *C* (with an applied bias of 1 V) from MC simulations and from our HD model.

Figure 14 shows the electron energy distribution in logarithmic scale as function of energy at some positions in devices *A*, *B*, and *C* (with a bias of 1 V). We note that MC data show, near the second junction, a *ballistic tail* which is partially reproduced by the HD simulation. This is particularly evident for device *A*, for which we show four points in proximity to the second junction.

We have verified that system (10) with closure (11), owing to the elevate values of moments (around the second junction), loses its hyperbolic character. For this reason, in our simulation we used expressions of G_Σ and G_S limited to second order, which make the hyperbolicity zone of the system much wider. In next section we will analyze the hyperbolic structure of system (10).

VI. ANALYSIS OF THE HYPERBOLICITY ZONE

In the one-dimensional case, by defining F_A the vector of independent variables, F_{Ax} the vector of the fluxes, and $S_A = R_A + P_A + \tilde{P}_A$ the source term, system (10) can be compactly written as

$$\frac{\partial F_A}{\partial t} + J_{AB} \frac{\partial F_B}{\partial x} = S_A, \quad (16)$$

where $J_{AB} = \partial F_{Ax} / \partial F_B$ is the Jacobian matrix of fluxes.

In the framework of extended thermodynamics, by using the entropy principle [which can be shown to be equivalent to the EMP (Ref. 28)] and the *concavity* of the entropy den-

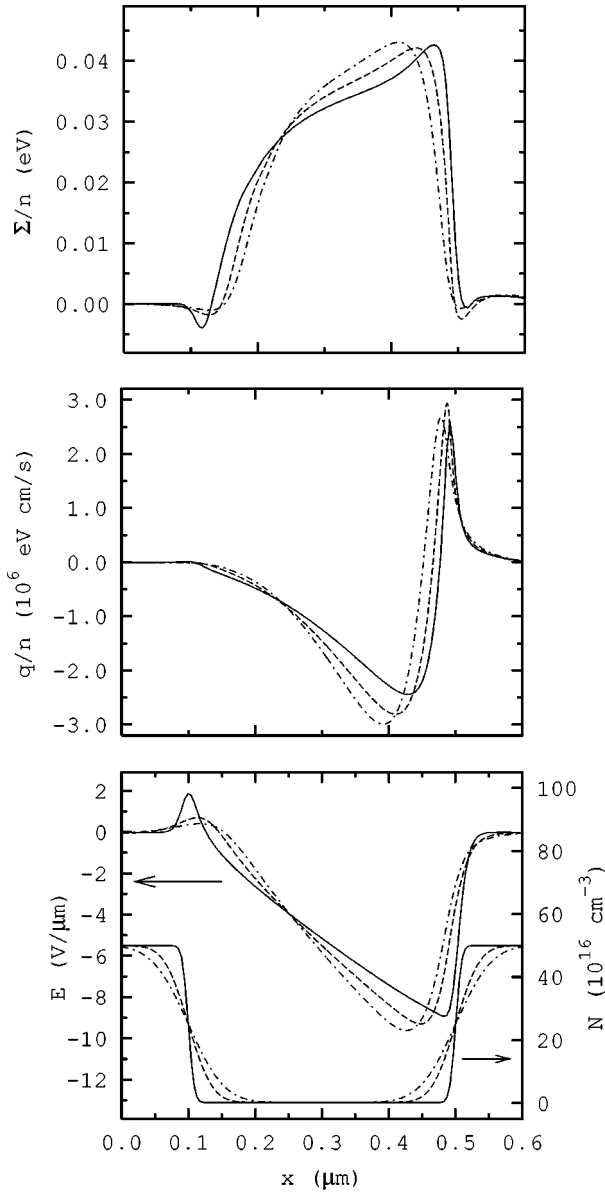


FIG. 6. Traceless momentum flux, heat flux, doping profiles, and electric field for devices *C* (solid line), *D* (dashed line), and *E* (dash-dotted line) with a 2 V bias.

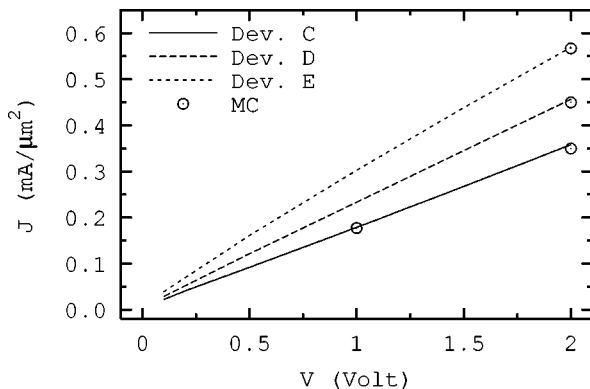


FIG. 7. Characteristic curves current density-bias for devices *C*, *D*, and *E* from the HD model and sample points from MC simulations.

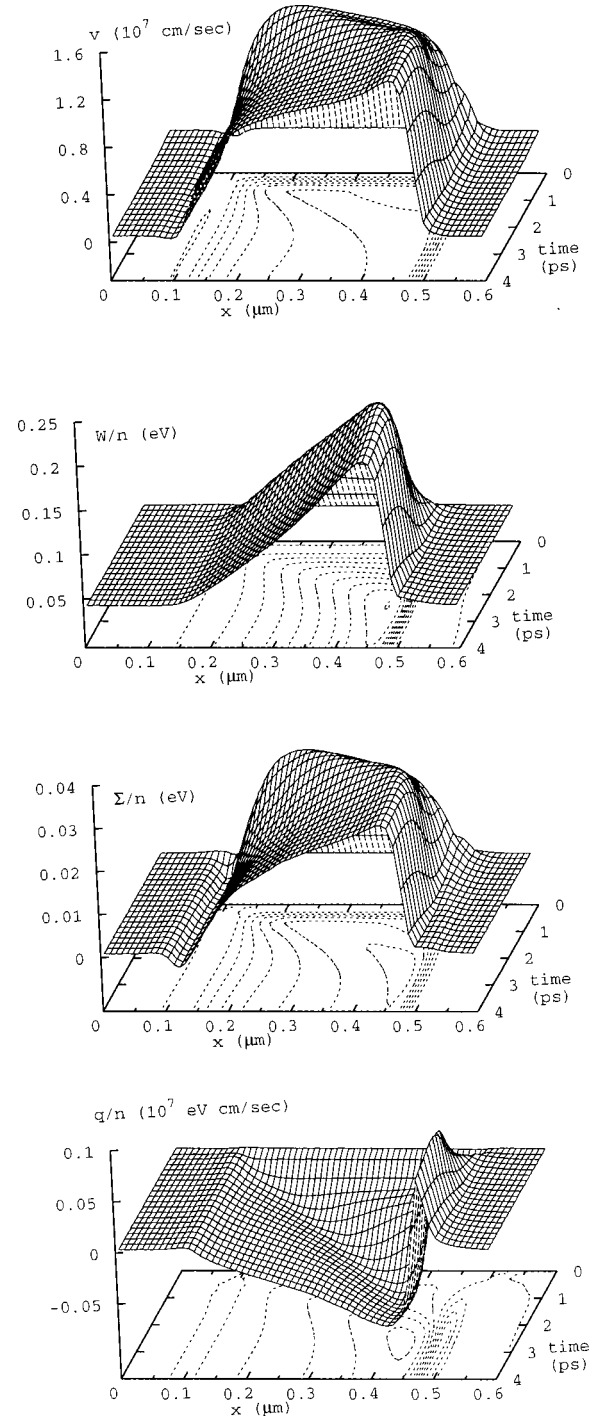


FIG. 8. Field values as function of position and time for device *C* with a 1 V bias.

sity h , it can be proved²² that the system (6) may be written in a symmetric hyperbolic form (in the sense of Friedrichs and Lax²⁹) inside a given neighborhood of the local equilibrium configuration. This property assures regular solutions with finite speeds of propagation and ensures also the applicability of the numerical scheme we have used. Since all the constitutive functions of system (10) (and the associated entropy density) have been obtained through a series expansion around local equilibrium, even the hyperbolicity zone does depend on this expansion. In this paragraph we intend to find the limits of hyperbolicity of the system, starting from an analysis of its characteristic speeds.

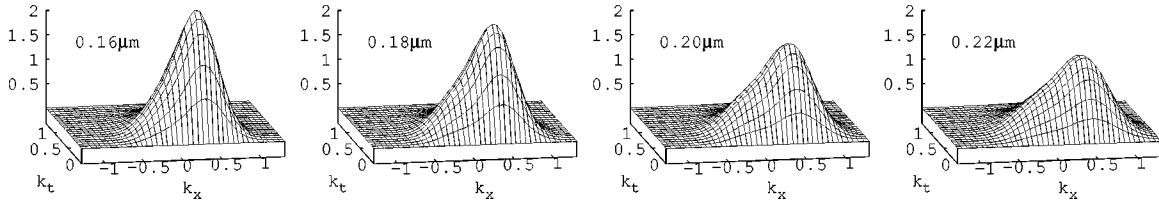


FIG. 9. Normalized distribution function f [see Eq. (14)] at different positions of device C with a 1 V bias. Wave vectors k_x and k_t are in units of 10^9 m^{-1} , f is in units of 10^{-18} m^2 .

The system is hyperbolic if the jacobian matrix of fluxes J has only real eigenvalues and a complete set of eigenvectors, so we should study the characteristic polynomial of J , that we write as

$$\lambda^5 + g_1 \lambda^4 + g_2 \lambda^3 + g_3 \lambda^2 + g_4 \lambda + g_5 = 0.$$

Here the g_i coefficients are function of the variables $\{n, v, p, \sigma, q\}$. In order to simplify our analysis, it is convenient to define a speed $c = \sqrt{p/nm^*}$ and the dimensionless quantities

$$\tilde{\lambda} = \frac{(\lambda - v)}{c}, \quad \tilde{v} = \frac{v}{c}, \quad \tilde{\sigma} = \frac{\sigma}{p}, \quad \tilde{q} = \frac{q}{c^3 nm^*}. \quad (17)$$

In so doing the polynomial assumes the simplified form

$$\tilde{\lambda}^5 + \tilde{g}_1 \tilde{\lambda}^4 + \tilde{g}_2 \tilde{\lambda}^3 + \tilde{g}_3 \tilde{\lambda}^2 + \tilde{g}_4 \tilde{\lambda} + \tilde{g}_5 = 0, \quad (18)$$

where the new coefficients \tilde{g}_i depend only on the three dimensionless variables $\{\tilde{v}, \tilde{\sigma}, \tilde{q}\}$ (see Appendix C for the explicit expressions) and they have a form that depends on the order of the series expansion of constitutive functions G_A . At local thermodynamic equilibrium we have $v = \sigma = q = 0$ and Eq. (18) simplifies to

$$\tilde{\lambda}^5 - \frac{26}{5} \tilde{\lambda}^3 + 3 \tilde{\lambda} = 0$$

with the following (real) roots:

$$\tilde{\lambda}_1 = 0, \quad \tilde{\lambda}_{2,3} = \pm \frac{\sqrt{65 + 5\sqrt{94}}}{5}, \quad \tilde{\lambda}_{4,5} = \pm \frac{\sqrt{65 - 5\sqrt{94}}}{5}.$$

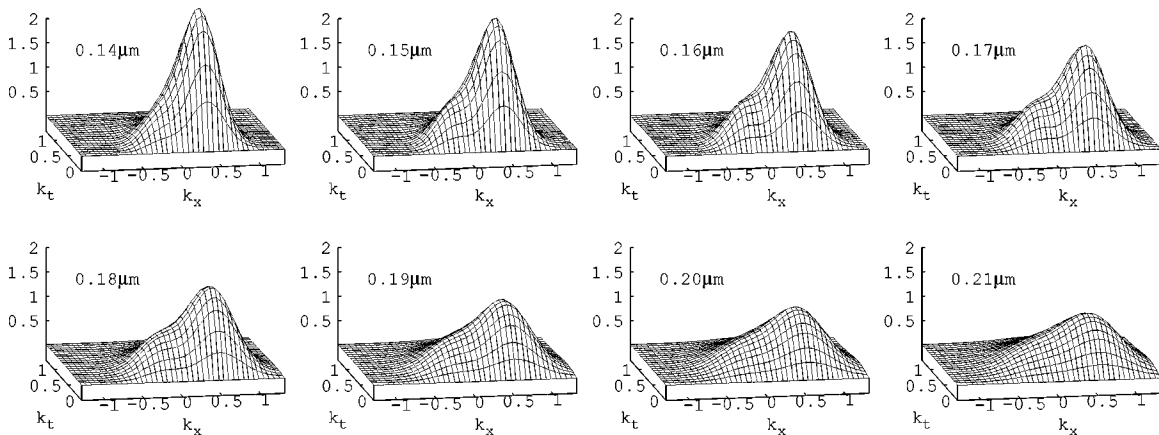


FIG. 10. Same quantities as for Fig. 9 with a 2 V bias. We observe that in nonequilibrium conditions the usual approximation of “displaced Maxwellian” (Ref. 3) cannot be considered effective.

We see then, that the system will be hyperbolic in a neighborhood of the equilibrium configuration in the three-dimensional space spanned by axes $\{\tilde{v}, \tilde{\sigma}, \tilde{q}\}$.

At first order the closure for functions G_A coincides with the usual gasdynamics one, so we will skip this case, already covered in the literature.³⁰ We have studied the hyperbolicity zone at second and third order through a numerical computation of the roots of the characteristic polynomial (18), by fixing values of $\tilde{\sigma}$ and representing in plane $\{\tilde{v}, \tilde{q}\}$ the regions with zero, two, or four complex conjugate roots. As shown in Figs. 15 and 16 the hyperbolicity zone is much wider for a second-order expansion of the G_A . For this reason we have used, for the simulations shown in this paper, the second-order closure, since we have noted that in several cases the strong nonequilibrium conditions lead the system outside the third-order hyperbolicity zone. In Fig. 17 we report, as an example, the dimensionless quantities $\{\tilde{v}, \tilde{\sigma}, \tilde{q}\}$ for device A as function of the position. We can observe that, while $\tilde{\sigma}$ changes by a little amount inside the device (in a range between -0.3 and 0.2) this is not the case of $\{\tilde{v}, \tilde{q}\}$. We see also [from the graphics of Fig. 16 corresponding to $\tilde{\sigma} = -0.4, 0, 0, 0.4$] that the hyperbolicity zone does not vary much for values of $\tilde{\sigma}$ close to zero. If we represent (see Fig. 16) the parametric curve $\{\tilde{v}(x), \tilde{q}(x)\}$ in the graphic corresponding to $\tilde{\sigma} = 0$, we can then observe, as we said at the end of the previous section, that the system, for some values of $\{\tilde{v}, \tilde{q}\}$ loses its hyperbolic character. This phenomenon is even more evident for devices in which the electric field reaches higher values.

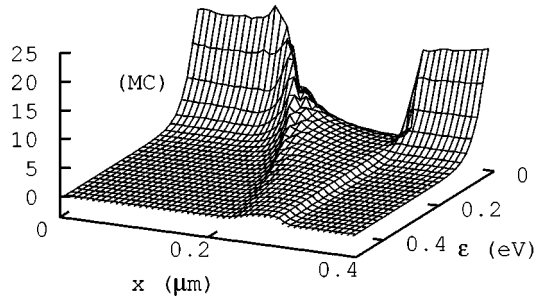
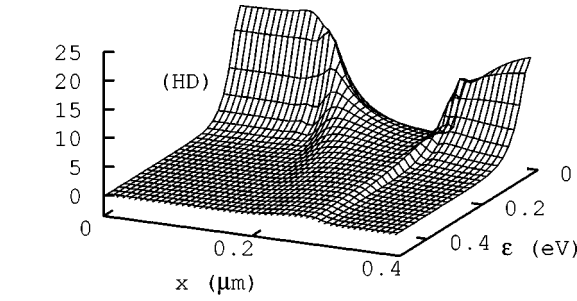


FIG. 11. Electron energy distribution normalized to unit [see Eq. (15)] as a function of position x for device A, from MC simulation and from the present HD model.

VII. NUMERICAL METHOD

System (10) is of the quasilinear hyperbolic type, and it is known that such systems can develop discontinuities of various kinds even if initial conditions are regular.³¹ This peculiarity requires us to use numerical methods capable of describing both the continuous and discontinuous regions of the solutions. In our case it is impossible to determine an analytic expression for the eigenvalues and eigenvectors of the Jacobian matrix of fluxes. This fact makes difficult the usage of common methods for hyperbolic equations, which require a knowledge of the characteristic structure of the system.³² For this reason we have used a generalization (for nonhomogeneous systems) of the *shock capturing* numerical procedure proposed by Nessyahu and Tadmor.³³ This method is based on a staggered Lax-Friedrichs scheme corrected by MUSCL-like interpolations.

The effect of source terms [right-hand side of Eqs. (10)] has been included in the algorithm through the following scheme. System (10) can be written, omitting for the sake of simplicity the index A , as

$$\frac{\partial F}{\partial t} + \frac{\partial G(F)}{\partial x} = S(F),$$

where $F = F_A$, $G = F_{Ax}$, $S = S_A$ are the vectors of, respectively, the macroscopic fields, their fluxes, and their production terms. Consider an equally spaced grid of N_c cells of width h and a constant time step k . Let F_j^n be the mean values of fields in cell j at time step n . Consider also a staggered grid, whose mean values are denoted by $F_{j+1/2}$. Starting from field values at time step n , we can first compute F and then G, S at an intermediate time step $n + 1/2$, and

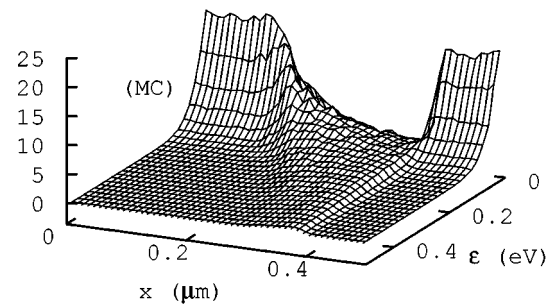
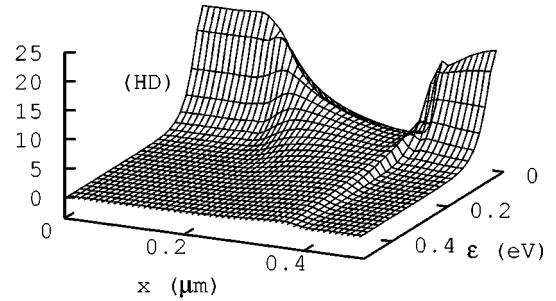


FIG. 12. Same quantities as for Fig. 11 for device B.

then obtain the fields at time step $n + 1$ considering time-centered derivatives. The resulting algorithm is globally of second order in time. The main steps of the algorithm are the following:

$$(a) \quad F_j^{n+(1/2)} = F_j^n - \frac{k}{2} \frac{G'(F_j^n)}{h} + \frac{k}{2} S(F_j^n),$$

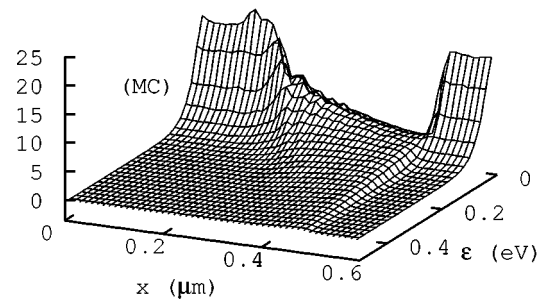
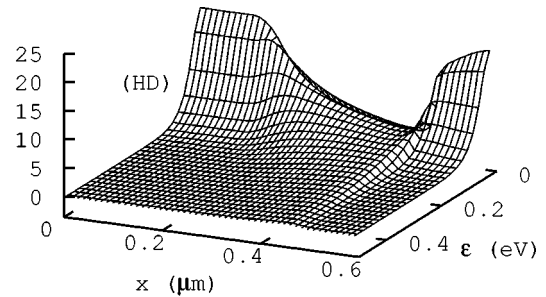


FIG. 13. Same quantities as for Fig. 11 for device C with a 1 V bias.

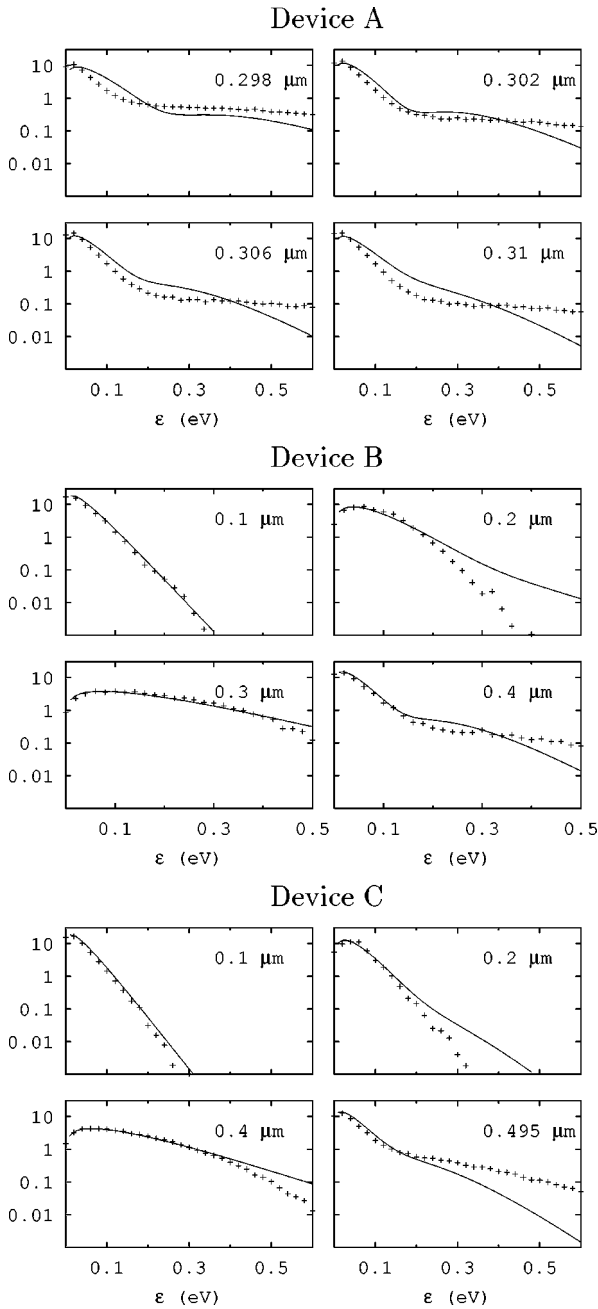


FIG. 14. MC (crosses) and HD (solid lines) electron energy distributions normalized to unit at various positions of devices A, B, and C (1 V).

$$(b) \quad G_j^{n+(1/2)} = G(F_j^{n+(1/2)}), \quad S_j^{n+(1/2)} = S(F_j^{n+(1/2)}),$$

$$(c) \quad F_{j+(1/2)}^{n+1} = \frac{1}{2}(F_j^n + F_{j+1}^n) + \frac{1}{8}(F_j'^n - F_{j+1}'^n) \\ + \frac{k}{2}(S_j^{n+(1/2)} + S_{j+1}^{n+(1/2)}) \\ + \frac{k}{h}(G_j^{n+(1/2)} - G_{j+1}^{n+(1/2)}),$$

where F'/h , G'/h are approximation of the gradients of F and G evaluated with a UNO scheme.³³ Electric field has

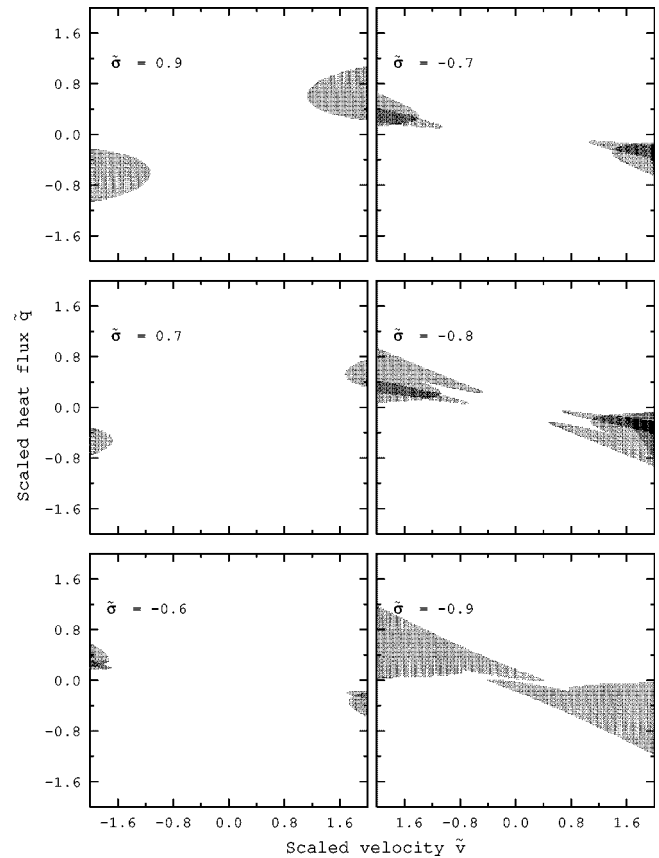


FIG. 15. Hyperbolicity zone for system (10) with a second-order closure for the fluxes. In the light gray and dark gray regions, the characteristic polynomial (18) of the Jacobian matrix has, respectively, two and four complex conjugate roots.

been self-consistently computed solving Poisson equation for the total spatial charge $e(N_D - n) = \epsilon \Delta \phi$, with $\epsilon = 11.7\epsilon_0$, at each time step.

VIII. CONCLUSIONS

We have shown that the entropy maximum principle allows us to create a closed hydrodynamic model containing *no free parameters* to describe transport phenomena in Si in strong nonequilibrium conditions. Our approach permits to determine a strongly nonlinear distribution function of carriers and, consequently, to calculate all the unknown constitutive functions by integrations of their kinetic expressions. The physical quantities of our model are then only those appearing in the scattering kernels, as happens for all kinetic models (MC, spherical harmonics, etc.). Our model, however, requires much smaller computational times. We think that this approach, based on the EMP and extended thermodynamics, opens the road to a series of hydrodynamic models that can show real advantages in the simulation of semiconductor devices. The power and generality of the method resides in the possibility of finding valid equations for the macroscopic quantities relative to a fluid, or a mixture of fluids, on the sole basis of the knowledge of the elementary microscopic interactions.

We underline that with the equations reported in this work and the quantities contained in the appendixes, it is possible to reproduce all our results, and also to perform other device

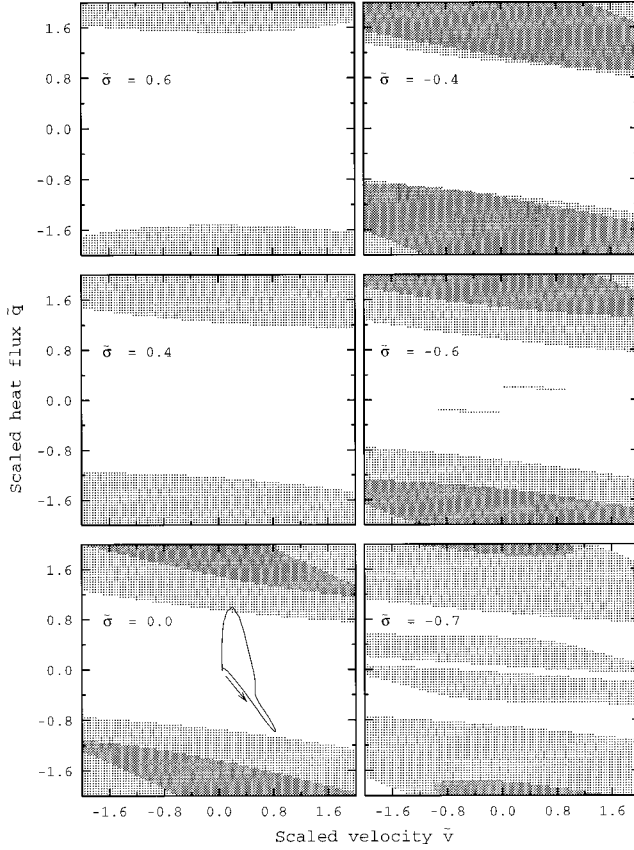


FIG. 16. Same representation of Fig. 15 for a third-order closure for fluxes. In the $\tilde{\sigma}=0.0$ figure we report the parametric curve of the values assumed by scaled fields $\{\tilde{v}(x), \tilde{q}(x)\}$ in device A [see also Fig. 17]. The arrow shows the direction of growth of the parameter x along the curve, which starts and ends near point $\{0,0\}$.

simulations with different doping profiles, biases, and lattice temperatures.

Regarding to the simulations shown in this paper, we make clear that, even if for this work we have developed only an one-dimensional code, our model is fully three dimensional, and a two-dimensional code is in progress.

By means of the entropy maximum principle our model can be extended both by taking into account further moments of the distribution function and by including a more detailed physical description (holes, realistic band structures, and other scattering processes). Many of these extensions have been already developed and they will be the subject of future papers.

ACKNOWLEDGMENTS

The authors thank O. Muscato for providing most of the MC data. This work has been partially supported by CNR

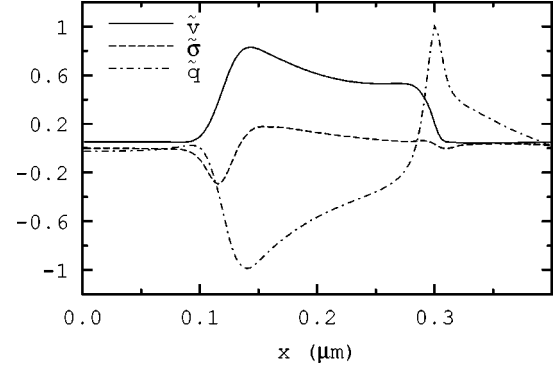


FIG. 17. Scaled fields (17) as function of position for device A.

Research Contract No. 96.03855.CT01.

APPENDIX A

Coefficients $\{\tilde{A}, \tilde{C}, \tilde{D}\}$, appearing in intravalley production terms (12), obtained starting from a third-order expansion in the nonequilibrium variables $\{v, \sigma, q\}$:

$$\begin{aligned} \tilde{A} &= \left(\frac{5p^2v}{n} + \frac{pq}{n} \right) + \left(\frac{p\sigma v}{n} - \frac{\sigma q}{5n} \right) + \left(\frac{pm^*v^3}{2} - \frac{2m^*vq^2}{5p} \right. \\ &\quad \left. - \frac{59m^*q^3}{125p^2} - \frac{11\sigma^2v}{56n} - \frac{3m^*v^2q}{10} - \frac{51\sigma^2q}{1400pn} \right), \\ \tilde{C} &= \left(\frac{5p^2\sigma}{2m^*n} \right) + \left(\frac{5p^2v^2}{3} + \frac{7q^2}{15} + \frac{2pqv}{3} + \frac{5p\sigma^2}{28m^*n} \right) \\ &\quad + \left(\frac{101q^2\sigma}{175p} + \frac{53v\sigma q}{210} + \frac{55pv^2\sigma}{84} - \frac{5\sigma^3}{112m^*n} \right), \\ \tilde{D} &= \left(q + \frac{5pv}{3} \right) + \left(\sigma v + \frac{\sigma q}{5p} \right) + \left(\frac{13m^*nvq^2}{25p^2} + \frac{82m^*nq^3}{125p^3} \right. \\ &\quad \left. + \frac{m^*v^3n}{2} + \frac{11\sigma^2v}{56p} + \frac{3m^*v^2qn}{10p} + \frac{23\sigma^2q}{200p^2} \right). \end{aligned}$$

Coefficients $\{A_i, B_i, C_i, D_i\}$, appearing in intervalley production terms (13), obtained starting from a third-order expansion in the nonequilibrium variables $\{v, \sigma, q\}$. Coefficients D_i can be expressed through A_i by means of the relation $D_{2i+1} = (p/n)A_{2i-1}$, $i=2, \dots, 6$, while for the remaining coefficients we have

$$\begin{aligned} A_3 &= \left(\frac{2p^2v}{n^2} - \frac{2pq}{n^2} \right) + \left(\frac{14\sigma q}{5n^2} - \frac{2p\sigma v}{n^2} \right) + \left(\frac{14m^*vq^2}{25pn} + \frac{11\sigma^2v}{4n^2} + \frac{21m^*v^2q}{5n} - \frac{279\sigma^2q}{100pn^2} + \frac{196m^*q^3}{125p^2n} - \frac{pm^*v^3}{n} \right), \\ A_5 &= \left(\frac{4pq}{5n^2} \right) + \left(\frac{4p\sigma v}{5n^2} - \frac{56\sigma q}{25n^2} \right) + \left(\frac{1053\sigma^2q}{250pn^2} - \frac{11\sigma^2v}{5n^2} + \frac{98m^*q^3}{625p^2n} + \frac{322m^*vq^2}{125pn} - \frac{84m^*v^2q}{25n} + \frac{2pm^*v^3}{5n} \right), \end{aligned}$$

$$A_7 = \left(\frac{8\sigma q}{25n^2} \right) + \left(\frac{4m^*q^3}{625p^2n} - \frac{1269\sigma^2q}{875pn^2} - \frac{208m^*vq^2}{125pn} + \frac{12m^*v^2q}{25n} + \frac{11\sigma^2v}{35n^2} \right),$$

$$A_9 = \left(\frac{24m^*vq^2}{125pn} - \frac{24m^*q^3}{125p^2n} + \frac{22\sigma^2q}{175pn^2} \right),$$

$$A_{11} = \left(\frac{16m^*q^3}{625p^2n} \right),$$

$$B_1 = \left(\frac{8p^3}{n^3} \right) + \left(\frac{8pm^*qv}{n^2} - \frac{4p^2m^*v^2}{n^2} + \frac{3p\sigma^2}{n^3} + \frac{16m^*q^2}{5n^2} \right) + \left(\frac{4pm^*v^2\sigma}{n^2} - \frac{\sigma^3}{n^3} - \frac{144m^*q^2\sigma}{25pn^2} - \frac{56m^*v\sigma q}{5n^2} \right),$$

$$B_3 = \left(\frac{8p^2m^*v^2}{3n^2} - \frac{8m^*q^2}{15n^2} - \frac{4p\sigma^2}{n^3} - \frac{32pm^*qv}{3n^2} \right) + \left(\frac{2\sigma^3}{n^3} + \frac{16m^*q^2\sigma}{75pn^2} + \frac{112m^*v\sigma q}{5n^2} - \frac{16pm^*v^2\sigma}{3n^2} \right),$$

$$B_5 = \left(\frac{32pm^*qv}{15n^2} - \frac{32m^*q^2}{15n^2} + \frac{4p\sigma^2}{5n^3} \right) + \left(\frac{2672m^*q^2\sigma}{375pn^2} - \frac{224m^*v\sigma q}{25n^2} - \frac{4\sigma^3}{5n^3} + \frac{16pm^*v^2\sigma}{15n^2} \right),$$

$$B_7 = \left(\frac{32m^*q^2}{75n^2} \right) + \left(\frac{64m^*v\sigma q}{75n^2} - \frac{896m^*q^2\sigma}{375pn^2} + \frac{8\sigma^3}{105n^3} \right),$$

$$B_9 = \left(\frac{64m^*q^2\sigma}{375pn^2} \right),$$

$$C_5 = \left(\frac{4p^2\sigma}{n^3} \right) + \left(\frac{8p^2m^*v^2}{3n^2} + \frac{56m^*q^2}{75n^2} - \frac{112pm^*qv}{15n^2} - \frac{2p\sigma^2}{n^3} \right) + \left(\frac{516m^*v\sigma q}{25n^2} - \frac{808m^*q^2\sigma}{375pn^2} - \frac{22pm^*v^2\sigma}{3n^2} + \frac{9\sigma^3}{2n^3} \right),$$

$$C_7 = \left(\frac{32pm^*qv}{15n^2} - \frac{32m^*q^2}{15n^2} + \frac{4p\sigma^2}{7n^3} \right) + \left(\frac{508m^*q^2\sigma}{75pn^2} - \frac{18\sigma^3}{7n^3} - \frac{336m^*v\sigma q}{25n^2} + \frac{44pm^*v^2\sigma}{21n^2} \right),$$

$$C_9 = \left(\frac{32m^*q^2}{75n^2} \right) + \left(\frac{176m^*v\sigma q}{105n^2} - \frac{8432m^*q^2\sigma}{2625pn^2} + \frac{2\sigma^3}{7n^3} \right),$$

$$C_{11} = \left(\frac{176m^*q^2\sigma}{525pn^2} \right).$$

APPENDIX B

Analytic expression of the distribution function $f(k_x, k_t, m_A(x, t))$ (14), normalized to unit:

$$f(k_x, k_t, m_A) = 2\pi k_t \left(\frac{\hbar^2}{2\pi m^* p} \right)^{3/2} \exp\left(-\frac{\hbar^2}{2m^* p} (k_x^2 + k_t^2) \right) \{ 1 + R_1 + R_2 k_x + R_3 k_x^2 + R_4 k_x^3 + R_5 (k_x^2 + k_t^2) + R_6 (k_x^2 + k_t^2) k_x \\ + R_7 (k_x^2 + k_t^2) k_x^2 + R_8 (k_x^2 + k_t^2) k_x^3 + R_9 (k_x^2 + k_t^2)^2 k_x + R_{10} (k_x^2 + k_t^2)^2 k_x^2 + R_{11} (k_x^2 + k_t^2)^2 k_x^3 + R_{12} (k_x^2 + k_t^2)^2 \\ \times (2k_x^2 - k_t^2) k_x^2 + R_{13} (2k_x^2 - k_t^2) + R_{14} (2k_x^2 - k_t^2) k_x + R_{15} (2k_x^2 - k_t^2) k_x^2 + R_{16} (k_x^2 + k_t^2) (2k_x^2 - k_t^2) \\ + R_{17} (k_x^2 + k_t^2) (2k_x^2 - k_t^2) k_x + R_{18} (k_x^2 + k_t^2) (2k_x^2 - k_t^2) k_x^2 + R_{19} (2k_x^2 - k_t^2)^2 + R_{20} (2k_x^2 - k_t^2)^2 k_x \\ + R_{21} (k_x^2 + k_t^2) (2k_x^2 - k_t^2)^2 k_x + R_{22} (2k_x^2 - k_t^2)^3 + R_{23} (k_x^2 + k_t^2)^3 k_x^3 \},$$

where the coefficients R_i have the following expressions:

$$R_1 = \frac{m^*n}{p^2} qv - \frac{1}{2} \frac{m^*n}{p} v^2 + \frac{3}{8} \frac{1}{p^2} \sigma^2 + \frac{2}{5} \frac{m^*n}{p^3} q^2 - \frac{1}{8} \frac{1}{p^3} \sigma^3 - \frac{18}{25} \frac{m^*n}{p^4} q^2 \sigma - \frac{7}{5} \frac{m^*n}{p^3} vq\sigma + \frac{1}{2} \frac{m^*n}{p^2} v^2 \sigma,$$

$$R_2 = \frac{\hbar}{m^*} \left\{ \frac{m^* n}{p} v - \frac{m^* n}{p^2} q + \frac{7}{5} \frac{m^* n}{p^3} \sigma q - \frac{m^* n}{p^2} \sigma v + \frac{7}{25} \frac{m^{*2} n^2}{p^4} v q^2 + \frac{11}{8} \frac{m^* n}{p^3} v \sigma^2 + \frac{21}{10} \frac{m^{*2} n^2}{p^3} v^2 q - \frac{279}{200} \frac{m^* n}{p^4} \sigma^2 q \right. \\ \left. + \frac{98}{125} \frac{m^{*2} n^2}{p^5} q^3 - \frac{1}{2} \frac{m^{*2} n^2}{p^2} v^3 \right\},$$

$$R_3 = \frac{\hbar^2}{m^{*2}} \left\{ \frac{1}{2} \frac{m^{*2} n^2}{p^2} v^2 + \frac{1}{2} \frac{m^{*2} n^2}{p^4} q^2 - \frac{m^{*2} n^2}{p^3} q v + \frac{12}{5} \frac{m^{*2} n^2}{p^4} v q \sigma - \frac{m^{*2} n^2}{p^3} v^2 \sigma - \frac{7}{5} \frac{m^{*2} n^2}{p^5} q^2 \sigma \right\},$$

$$R_4 = \frac{\hbar^3}{m^{*3}} \left\{ \frac{1}{2} \frac{m^{*3} n^3}{p^5} v q^2 - \frac{1}{2} \frac{m^{*3} n^3}{p^4} v^2 q - \frac{1}{6} \frac{m^{*3} n^3}{p^6} q^3 + \frac{1}{6} \frac{m^{*3} n^3}{p^3} v^3 \right\},$$

$$R_5 = \frac{\hbar^2}{m^{*2}} \left\{ -\frac{1}{5} \frac{m^{*2} n^2}{p^4} q^2 - \frac{1}{4} \frac{m^* n}{p^3} \sigma^2 - \frac{1}{3} \frac{m^{*2} n^2}{p^3} q v + \frac{1}{8} \frac{m^* n}{p^4} \sigma^3 + \frac{12}{25} \frac{m^{*2} n^2}{p^5} q^2 \sigma + \frac{3}{5} \frac{m^{*2} n^2}{p^4} v q \sigma \right\},$$

$$R_6 = \frac{\hbar^3}{m^{*3}} \left\{ \frac{1}{5} \frac{m^{*2} n^2}{p^3} q - \frac{9}{25} \frac{m^{*2} n^2}{p^4} \sigma q + \frac{673}{1000} \frac{m^{*2} n^2}{p^5} \sigma^2 q + \frac{27}{625} \frac{m^{*3} n^3}{p^6} q^3 + \frac{1}{3} \frac{m^{*3} n^3}{p^5} v q^2 - \frac{1}{4} \frac{m^{*2} n^2}{p^4} v \sigma^2 - \frac{13}{30} \frac{m^{*3} n^3}{p^4} v^2 q \right\},$$

$$R_7 = \frac{\hbar^4}{m^{*4}} \left\{ \frac{1}{5} \frac{m^{*3} n^3}{p^4} q v - \frac{1}{5} \frac{m^{*3} n^3}{p^5} q^2 - \frac{14}{25} \frac{m^{*3} n^3}{p^5} v q \sigma + \frac{16}{25} \frac{m^{*3} n^3}{p^6} q^2 \sigma \right\},$$

$$R_8 = \frac{\hbar^5}{m^{*5}} \left\{ \frac{1}{10} \frac{m^{*4} n^4}{p^7} q^3 + \frac{1}{10} \frac{m^{*4} n^4}{p^5} v^2 q - \frac{1}{5} \frac{m^{*4} n^4}{p^6} v q^2 \right\},$$

$$R_9 = \frac{\hbar^5}{m^{*5}} \left\{ -\frac{1}{25} \frac{m^{*4} n^4}{p^7} q^3 - \frac{1}{20} \frac{m^{*3} n^3}{p^6} \sigma^2 q - \frac{1}{15} \frac{m^{*4} n^4}{p^6} v q^2 \right\},$$

$$R_{10} = \frac{\hbar^6}{m^{*6}} \left\{ \frac{1}{50} \frac{m^{*4} n^4}{p^6} q^2 - \frac{9}{125} \frac{m^{*4} n^4}{p^7} q^2 \sigma \right\},$$

$$R_{11} = \frac{\hbar^7}{m^{*7}} \left\{ -\frac{1}{50} \frac{m^{*5} n^5}{p^8} q^3 + \frac{1}{50} \frac{m^{*5} n^5}{p^7} v q^2 \right\},$$

$$R_{12} = \frac{1}{200} \frac{\hbar^8 n^5}{m^{*3} p^8} q^2 \sigma,$$

$$R_{13} = \frac{\hbar^2}{m^{*2}} \left\{ \frac{1}{4} \frac{m^* n}{p^2} \sigma - \frac{3}{25} \frac{m^{*2} n^2}{p^4} q^2 - \frac{2}{15} \frac{m^{*2} n^2}{p^3} q v - \frac{1}{8} \frac{m^* n}{p^3} \sigma^2 + \frac{83}{250} \frac{m^{*2} n^2}{p^5} q^2 \sigma + \frac{49}{100} \frac{m^{*2} n^2}{p^4} v q \sigma \right. \\ \left. - \frac{1}{8} \frac{m^{*2} n^2}{p^3} v^2 \sigma + \frac{9}{32} \frac{m^* n}{p^4} \sigma^3 \right\},$$

$$R_{14} = \frac{\hbar^3}{m^{*3}} \left\{ \frac{1}{4} \frac{m^{*2} n^2}{p^3} \sigma v - \frac{1}{4} \frac{m^{*2} n^2}{p^4} \sigma q + \frac{1}{75} \frac{m^{*3} n^3}{p^5} v q^2 - \frac{2}{15} \frac{m^{*3} n^3}{p^4} v^2 q + \frac{3}{25} \frac{m^{*3} n^3}{p^6} q^3 - \frac{3}{8} \frac{m^{*2} n^2}{p^4} v \sigma^2 + \frac{19}{40} \frac{m^{*2} n^2}{p^5} \sigma^2 q \right\},$$

$$R_{15} = \frac{\hbar^4}{m^{*4}} \left\{ \frac{1}{8} \frac{m^{*3} n^3}{p^4} v^2 \sigma + \frac{1}{8} \frac{m^{*3} n^3}{p^6} q^2 \sigma - \frac{1}{4} \frac{m^{*3} n^3}{p^5} v q \sigma \right\},$$

$$R_{16} = \frac{\hbar^4}{m^{*4}} \left\{ -\frac{1}{20} \frac{m^{*3} n^3}{p^6} q^2 \sigma - \frac{1}{16} \frac{m^{*2} n^2}{p^5} \sigma^3 - \frac{1}{12} \frac{m^{*3} n^3}{p^5} v q \sigma \right\},$$

$$R_{17} = \frac{\hbar^5}{m^{*5}} \left\{ \frac{1}{20} \frac{m^{*3} n^3}{p^5} \sigma q - \frac{3}{125} \frac{m^{*4} n^4}{p^7} q^3 - \frac{2}{75} \frac{m^{*4} n^4}{p^6} v q^2 - \frac{23}{200} \frac{m^{*3} n^3}{p^6} \sigma^2 q \right\},$$

$$R_{18} = \frac{\hbar^6}{m^{*6}} \left\{ -\frac{1}{20} \frac{m^{*4} n^4}{p^7} q^2 \sigma + \frac{1}{20} \frac{m^{*4} n^4}{p^6} v q \sigma \right\},$$

$$R_{19} = \frac{\hbar^4}{m^{*4}} \left\{ \frac{1}{32} \frac{m^{*2} n^2}{p^4} \sigma^2 - \frac{3}{100} \frac{m^{*3} n^3}{p^6} q^2 \sigma - \frac{1}{30} \frac{m^{*3} n^3}{p^5} v q \sigma - \frac{1}{32} \frac{m^{*2} n^2}{p^5} \sigma^3 \right\},$$

$$R_{20} = \frac{\hbar^5}{m^{*5}} \left\{ \frac{1}{32} \frac{m^{*3} n^3}{p^5} v \sigma^2 - \frac{1}{32} \frac{m^{*3} n^3}{p^6} \sigma^2 q \right\},$$

$$R_{21} = \frac{1}{160} \frac{\hbar^7}{m^{*3}} \frac{n^4}{p^7} \sigma^2 q, \quad R_{22} = \frac{1}{384} \frac{\hbar^6}{m^{*3}} \frac{n^3}{p^6} \sigma^3, \quad R_{23} = \frac{1}{750} \frac{\hbar^9}{m^{*3}} \frac{n^6}{p^9} q^3.$$

Analytic expression of the electron energy distribution $f(\varepsilon(k), m_A(x, t))$ (15), normalized to unit:

$$\begin{aligned} f(\varepsilon, m_A) = & \frac{2}{\sqrt{\pi}} \left(\frac{n}{p} \right)^{3/2} \varepsilon^{1/2} \exp\left(-\frac{n}{p} \varepsilon \right) \left\{ 1 + \left[\frac{2}{5} \frac{m^* n}{p^3} q^2 - \frac{1}{2} \frac{m^* n}{p} v^2 + \frac{3}{8} \frac{1}{p^2} \sigma^2 + \frac{m^* n}{p^2} q v + \left(\frac{1}{3} \frac{m^* n^2}{p^2} v^2 - \frac{1}{15} \frac{m^* n^2}{p^4} q^2 \right. \right. \right. \\ & \left. \left. - \frac{1}{2} \frac{n}{p^3} \sigma^2 - \frac{4}{3} \frac{m^* n^2}{p^3} q v \right) \varepsilon + \left(\frac{4}{15} \frac{m^* n^3}{p^4} q v - \frac{4}{15} \frac{m^* n^3}{p^5} q^2 + \frac{1}{10} \frac{n^2}{p^4} \sigma^2 \right) \varepsilon^2 + \frac{4}{75} \frac{m^* n^4}{p^6} q^2 \varepsilon^3 \right] \\ & + \left[\frac{1}{2} \frac{m^* n}{p^2} v^2 \sigma - \frac{18}{25} \frac{m^* n}{p^4} q^2 \sigma - \frac{1}{8} \frac{1}{p^3} \sigma^3 - \frac{7}{5} \frac{m^* n}{p^3} v \sigma q \right. \\ & + \left(\frac{2}{75} \frac{m^* n^2}{p^5} q^2 \sigma + \frac{14}{5} \frac{m^* n^2}{p^4} v \sigma q + \frac{1}{4} \frac{n}{p^4} \sigma^3 - \frac{2}{3} \frac{m^* n^2}{p^3} v^2 \sigma \right) \varepsilon \\ & + \left(\frac{334}{375} \frac{m^* n^3}{p^6} q^2 \sigma - \frac{28}{25} \frac{m^* n^3}{p^5} v \sigma q - \frac{1}{10} \frac{n^2}{p^5} \sigma^3 + \frac{2}{15} \frac{m^* n^3}{p^4} v^2 \sigma \right) \varepsilon^2 \\ & \left. \left. + \left(\frac{8}{75} \frac{m^* n^4}{p^6} v \sigma q - \frac{112}{375} \frac{m^* n^4}{p^7} q^2 \sigma + \frac{1}{105} \frac{n^3}{p^6} \sigma^3 \right) \varepsilon^3 + \frac{8}{375} \frac{m^* n^5}{p^8} q^2 \sigma \varepsilon^4 \right] \right\}. \end{aligned}$$

APPENDIX C

We report in the following the coefficients of the characteristic polynomial (18) of the Jacobian matrix of fluxes, with closures for the constitutive functions $\{G_\Sigma, G_S\}$ of second and third order.

For a second-order closure we have

$$\tilde{g}_1 = \frac{36}{25} \tilde{v} \tilde{\sigma} - \frac{184}{25} \tilde{q},$$

$$\tilde{g}_2 = \frac{96}{125} \tilde{q} \tilde{v} - \frac{36}{25} \tilde{\sigma}^2 - \frac{166}{25} \tilde{\sigma} + \frac{19 \cdot 684}{1875} \tilde{q}^2 - \frac{24}{25} \tilde{v} \tilde{q} \tilde{\sigma} - \frac{26}{5},$$

$$\tilde{g}_3 = -\frac{1776}{625} \tilde{q}^3 + \frac{48}{25} \tilde{q} \tilde{\sigma}^2 + \frac{2484}{125} \tilde{q} \tilde{\sigma} - \frac{108}{25} \tilde{v} \tilde{\sigma} - \frac{108}{25} \tilde{\sigma}^2 \tilde{v} + \frac{468}{25} \tilde{q},$$

$$\tilde{g}_4 = \frac{216}{125} \tilde{v} \tilde{q} \tilde{\sigma}^2 - \frac{1776}{625} \tilde{q}^2 \tilde{\sigma}^2 - \frac{8292}{625} \tilde{\sigma} \tilde{q}^2 - \frac{1392}{125} \tilde{q}^2 + \frac{216}{125} \tilde{v} \tilde{q} \tilde{\sigma} + 3 \tilde{\sigma}^2 + 6 \tilde{\sigma} + 3,$$

$$\tilde{g}_5 = -\frac{24}{25} \tilde{q} \tilde{\sigma}^3 - \frac{108}{25} \tilde{q} \tilde{\sigma}^2 - \frac{144}{25} \tilde{q} \tilde{\sigma} - \frac{12}{5} \tilde{q}.$$

For the third-order closure we have

$$\tilde{g}_1 = -\frac{184}{25} \tilde{q} - \frac{118}{125} \tilde{q} \tilde{\sigma} + \frac{816}{625} \tilde{v} \tilde{q}^2 - \frac{99}{125} \tilde{v} \tilde{\sigma}^2,$$

$$\begin{aligned}
\tilde{g}_2 &= -\frac{264}{3125} \tilde{v} \tilde{q} \tilde{\sigma}^2 - \frac{128}{78} \frac{928}{125} \tilde{q}^4 - \frac{528}{625} \tilde{v} \tilde{q} \tilde{\sigma} + \frac{5324}{625} \tilde{q}^2 + \frac{99}{125} \tilde{\sigma}^3 - \frac{42}{15} \frac{976}{625} \tilde{v} \tilde{q}^3 - \frac{67}{9375} \frac{288}{125} \tilde{q}^2 \tilde{\sigma} - \frac{81}{125} \tilde{\sigma}^2 - \frac{46}{15} \frac{926}{625} \tilde{q}^2 \tilde{\sigma}^2 - \frac{166}{25} \tilde{\sigma} - \frac{26}{5}, \\
\tilde{g}_3 &= \frac{1608}{625} \tilde{q} \tilde{\sigma}^2 - \frac{2448}{625} \tilde{v} \tilde{q}^2 + \frac{20}{15} \frac{856}{625} \tilde{q}^3 \tilde{\sigma}^2 + \frac{19}{15} \frac{584}{625} \tilde{v} \tilde{q}^4 + \frac{85}{78} \frac{952}{125} \tilde{q}^5 + \frac{27}{15} \frac{704}{625} \tilde{q}^3 \tilde{\sigma} + \frac{297}{125} \tilde{\sigma}^3 \tilde{v} + \frac{297}{125} \tilde{v} \tilde{\sigma}^2 - \frac{3036}{3125} \tilde{q} \tilde{\sigma}^3 - \frac{13}{3125} \frac{776}{125} \tilde{q}^3 - \frac{2448}{625} \tilde{v} \tilde{q}^2 \tilde{\sigma} \\
&\quad + \frac{2556}{125} \tilde{q} \tilde{\sigma} + \frac{468}{25} \tilde{q}, \\
\tilde{g}_4 &= \frac{26}{15} \frac{112}{625} \tilde{q}^4 + \frac{2376}{3125} \tilde{q} \tilde{v} \tilde{\sigma}^3 + \frac{53}{15} \frac{856}{625} \tilde{q}^3 \tilde{v} \tilde{\sigma} + \frac{38}{3125} \frac{664}{125} \tilde{q}^2 \tilde{\sigma}^2 - \frac{1392}{125} \tilde{q}^2 + \frac{11}{3125} \frac{424}{125} \tilde{v} \tilde{q}^3 + \frac{20}{15} \frac{856}{625} \tilde{q}^2 \tilde{\sigma}^4 + \frac{132}{15} \frac{924}{625} \tilde{q}^2 \tilde{\sigma}^3 - \frac{2616}{625} \tilde{q}^2 \tilde{\sigma} + \frac{68}{78} \frac{544}{125} \tilde{q}^4 \tilde{\sigma} \\
&\quad + \frac{2376}{3125} \tilde{q} \tilde{\sigma}^4 \tilde{v} + 3 \tilde{\sigma}^2 + 6 \tilde{\sigma} + 3, \\
\tilde{g}_5 &= -\frac{95}{78} \frac{744}{125} \tilde{q}^5 - \frac{6528}{15} \frac{625}{625} \tilde{q}^4 \tilde{v} \tilde{\sigma} - \frac{171}{234} \frac{904}{375} \tilde{q}^5 \tilde{\sigma} + \frac{252}{125} \tilde{q} \tilde{\sigma}^2 + \frac{132}{125} \tilde{q} \tilde{\sigma}^4 - \frac{544}{625} \tilde{q}^3 \tilde{\sigma}^2 - \frac{1088}{625} \tilde{q}^3 - \frac{1632}{625} \tilde{q}^3 \tilde{\sigma} - \frac{6528}{15} \frac{625}{625} \tilde{v} \tilde{q}^4 + \frac{474}{125} \tilde{q} \tilde{\sigma}^3 - \frac{78}{25} \tilde{q} \tilde{\sigma} \\
&\quad - \frac{12}{5} \tilde{q},
\end{aligned}$$

-
- ¹M. Fischetti and S. Laux, Phys. Rev. B **48**, 2244 (1993).
²C. Jacoboni and L. Reggiani, Rev. Mod. Phys. **55**, 645 (1993).
³R. Stratton, Phys. Rev. **126**, 2002 (1962).
⁴A. Gnudi, D. Ventura, and G. Baccarani, IEEE Trans. Comput.-Aided Des. **12**, 1706 (1993).
⁵S. E. Laux and M. V. Fischetti, *Transport Models for Advanced Device Simulation—Truth or Consequence? Proceedings of the 1995 Bipolar/EMOS Circuits and Technology Meeting*, (IEEE, New York, 1995).
⁶T. Tang, S. Ramaswamy, and J. Nam, IEEE Trans. Electron Devices **40**, 1469 (1993).
⁷P. Falsaperla and M. Trovato, in *A Hydrodynamic Model for Transport in Semiconductors Without Free Parameters*, edited by G. W. Zobrist, Proceedings of IWCE-5 (to be published in VLSI Design).
⁸W. Hansch and M. Miura-Mattausch, J. Appl. Phys. **60**, 650 (1986).
⁹M. Rudan, F. Odeh, and J. White, Int. J. Comput. Math. Electr. Electron Eng. **6**, 151 (1987).
¹⁰C. L. Gardner, J. W. Jerome, and D. J. Rose, IEEE Trans. Cad. **8**, 501 (1989).
¹¹C. L. Gardner, IEEE Trans. Electron Devices **38**, 392 (1991).
¹²D. L. Woolard, H. Tian, R. J. Trew, M. A. Littlejohn, and W. Kim, Phys. Rev. B **44**, 11 119 (1991).
¹³R. Thoma, A. Emunds, B. Meinerzhagen, H. J. Peifer, and W. L. Engl, IEEE Trans. Electron Devices **38**, 1343 (1991).
¹⁴A. M. Anile and O. Muscato, Phys. Rev. B **51**, 16 728 (1995).
¹⁵Here and in the following symbol $A_{\langle ij \rangle}$ denotes the traceless part of a symmetric tensor A , i.e., $A_{\langle ij \rangle} = A_{ij} - \frac{1}{3} \delta_{ij} \text{Tr}(A)$.
¹⁶*Maximum Entropy and Bayesian Methods*, edited by W. Grandy (Kluwer, Dordrecht, 1991).
¹⁷C. D. Levermore, J. Stat. Phys. **83**, 331 (1996).
¹⁸E. T. Jaynes, Phys. Rev. **106**, 620 (1957).
¹⁹M. Tribus, *Thermostatistics and Thermodynamics* (Van Nostrand, Princeton, 1961).
²⁰*The Maximum Entropy Formalism*, edited by R. D. Levine and M. Tribus (MIT, Cambridge, MA, 1979).
²¹E. T. Jaynes, *Papers on Probability, Statistics, and Statistical Physics*, edited by R. D. Rosenkrantz (Reidel, Dordrecht, 1983).
²²I. Müller and T. Ruggeri, *Extended Thermodynamics* (Springer-Verlag, Berlin, 1993).
²³D. Jou, J. Casas-Vasquez, and G. Lebon, *Extended Irreversible Thermodynamics* (Springer-Verlag, Berlin, 1993).
²⁴A. M. Anile and M. Trovato, Phys. Lett. A **230**, 387 (1997).
²⁵E. Fatemi, J. Jerome, S. Osher, IEEE Trans. Comput.-Aided Des. **10**, 232 (1991).
²⁶The MC code DAMOCLES has been developed by M. V. Fischetti and S. E. Laux at the IBM T. J. Watson Laboratories.
²⁷M. Fischetti, IEEE Trans. Electron Devices **38**, 634 (1991).
²⁸W. Dreyer, J. Phys. A **20**, 6505 (1987).
²⁹K. O. Friedrichs and P. D. Lax, Proc. Natl. Acad. Sci. USA **68**, 1686 (1971).
³⁰The hyperbolicity region corresponding to a first-order closure of the fluxes has been widely studied in Ref. 22. We note only that in this case the analysis is reduced to the plane $\{\tilde{\sigma}, \tilde{q}\}$, since the coefficients of the characteristic polynomial do not depend on \tilde{v} .
³¹A. Jeffrey, in *Quasilinear Hyperbolic Systems and Waves*, edited by A. Jeffrey, Research Notes in Mathematics (Pitman, San Francisco, 1976).
³²R. Leveque, *Numerical Methods for Conservation Laws* (Birkhäuser, Basel, 1990).
³³H. Nessyahu and E. Tadmor, J. Comput. Phys. **87**, 408 (1990).